Proceedings of the ASME 2017 International Design Engineering Technical Conferences and Computers and Information in Engineering Conference
IDETC/CIE 2017
August 6-9, 2017, Cleveland, Ohio, USA

DETC2017-67458

MODELING LENGTH EFFECTS OF BRAIDED PNEUMATIC ACTUATORS

Alexander J Hunt
Portland State University
Portland, Oregon, U.S.A.

Alexander Graber-Tilton
Case Western Reserve University
Cleveland, Ohio, U.S.A.

Roger D Quinn
Case Western Reserve University
Cleveland, Ohio, U.S.A.

ABSTRACT

Braided pneumatic actuators (BPAs) are attractive for use in bio-robots because they offer many muscle-like properties, especially when compared to most other commercially available robotic actuators. Unfortunately, the same properties that make these actuators similar to muscles make them more difficult to control. One such actuator manufactured by Festo, the MXAM-10-AA, is frequently utilized in robotics because of its commercial availability, durability, and force capability. Although models for BPAs exist, the properties that make this actuator more durable also make its behavior less like other braided pneumatic actuators, especially for shorter actuator lengths. Length specific models that do exist for Festo fluidic muscles have numerous parameters that can only be found experimentally by taking hundreds to thousands of data points and performing a lengthy optimization process to fit parameter values for each actuator in the system. This lack of generalizability makes it difficult to build a new robot and begin testing new control systems without significant startup time and cost. The key contribution of this work is the development of a generalizable actuator model that accounts for the geometry and limitations of the actuator at shorter lengths. This empirical model relates internal pressure, strain, stretching or contracting state, and applied force on the MXAM-10-AA actuator. The model is scalable to different length actuators by measuring their resting length at zero pressure and their minimum contraction length at maximum air pressure, and can be used for feedforward length control. The model is evaluated on a robot leg with three joints and 6 actuators, each with different length. The developed controller, using the actuator model, controls the joints to within ± 3 degrees of the desired position for different desired torques only using internal actuator pressure feedback. We also demonstrate control speed by cycling a joint over 40 degrees of rotation at varying frequencies.

INTRODUCTION

Though muscles are inefficient compared to most robot actuators (electric motors, hydraulic cylinders, etc.) [1], animal control of muscles has resulted in more efficient and agile locomotion over a wide variety of terrains than any current legged robot. This is because the combination of muscles with tendons creates a compliant actuation system with many advantages. Compliance allows energy to be stored and returned to the system during repetitive tasks such as walking and running. Legs with compliant joints are also able to conform to the surrounding environment. This makes them safer than non-compliant actuators, without the need for complex controllers to absorb perturbations. The compliant structure of the muscle-tendon system also requires less energy to maintain stability when suddenly perturbed [2, 3]. Another advantage to muscular systems is that joint compliance can be varied by activating antagonistic muscles [4]. This variable compliance allows joints to be tuned to work more effectively for a variety of speeds [5], ground stiffness [6], and changes in environment [7]. These advantages have led to the development of several variably compliant actuator systems [8–11].

Biological control systems (neural systems) evolved in tandem with muscles to control them effectively. With advances in neurobiology, research into biologically and neurologically derived controllers has increased significantly in recent years [12–17]. Many of these control systems take advantage of the compliant nature of the tendon-muscular system. To fully test these control theories, robots with biomechanical properties similar to animals need be developed [18].

Braided pneumatic actuators (BPAs), also known as McKibben Actuators and Rubbertuators, have been explored in the robotic community for many decades [19–22]. A BPA consists of an interwoven mesh combined with a bladder that changes shape due to changes in internal pressure. When pressure inside an unrestrained actuator is increased, the diameter of the actuator increases, causing the ends to contract (Fig. 1). If the ends are restrained and the actuator cannot contract, the tensile force increases with pressure. The Festo BPA is similar, but the mesh is integrated within the tube.

Figure 1. The Festo BPA in a relaxed, uninflated state (A), and a contracted, pressurized state (B).

BPAs offer the most similar gross properties to that of muscles compared to most other robotic actuators. BPAs are similar to muscles in that they are compliant and they can only effectively pull to provide force, requiring at least two antagonistic actuators to be positioned on each joint to provide torque in both directions. These actuators can be operated independently, like muscles, and their operation can provide variable joint compliance around a joint. BPAs have been used on a variety of robots [23, 24]. However, the advantages of compliance lead to a lack of precision, and these robots largely underperform compared to their hydraulic or electric counterparts in terms of positional accuracy. Length-pressure-force relationships of BPAs are complex. Additionally, hysteresis and creep have significant effects that can alter output force by 10% [25, 26]. This makes feed-forward control of pressure to produce desired positions or torques not easy to compute. Additionally, in order to control a single joint, at least two parallel actuators must be controlled, compounding problems of uncertainty.

To avoid this complexity, many controllers use joint angle feedback transformed into valve control [27–30]. However, these control methods can suffer from delays and may be unable to respond quickly enough for robust robotic systems. Modeling BPAs and creating feedforward controllers has resulted in more responsive systems capable of achieving speeds that more closely match animal movements [31–34]. However, these models have parameters that must be found experimentally by taking a large amount of data and performing a lengthy optimization process for every actuator in the system. In some cases, different parameters are even found between filling and emptying the same actuator with compressed air. This lack of generalizability makes it difficult to build a new robot and begin testing of new control systems without significant startup time and cost.

This paper develops an empirically derived generalizable model of the commercially available10 mm Festo fluidic muscle for implementing feedforward control methods. Only the strain of the actuator under 620 kpa (maximum air pressure) and its resting length with no load (2 length data points) need to be experimentally measured for a 10mm Festo actuator of any length to be modeled. The model can then be used to provide control of length and force with only internal pressure feedback. This model is validated on a three joint, six actuator robot limb.

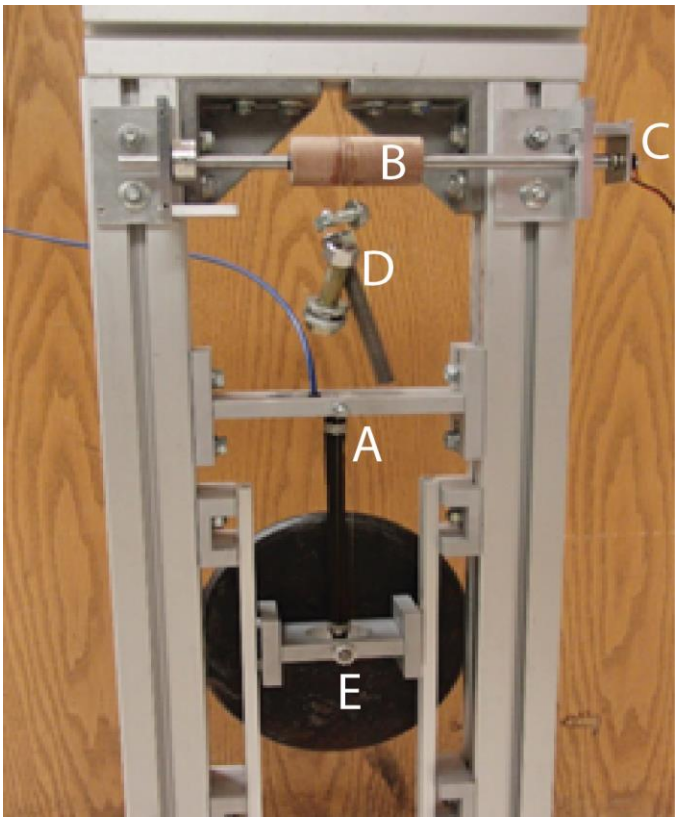

Figure 2. Test stand used in data collection. Actuator (A) length changes are transformed into shaft rotation (B) and collected by a potentiometer (C). Shaft counterweight ensures string remains taught (D). Weights are hung incrementally on the end of the actuator (E).

MATERIALS AND METHODS

Data Collection

Data was collected on 6 actuators to develop and test the model fit. These actuators are 10 mm Festo MXAM-10-AA and have resting lengths of 15.3, 18.3, 18.9, 19.5, 27.3, and 28.1 cm from attachment point to attachment point. Each actuator was secured on a vertical test stand (Fig. 2) with the top fixed and the bottom attached to a weighted moving slider. Actuator length data was collected using a Vishay Spectrol 140-0-0-103 potentiometer connected to the moving plate via Kevlar thread wrapped around a 3.18 cm shaft. Pressure was measured using a Freescale MPX5700GP gauge pressure sensor. Data was collected with Labview 2014 via a sbRIO-9602 and processed in Matlab 2014b.

Testing Procedure: The actuator began at 0 gauge pressure and the inlet valve was opened for 10 ms from a 650 kPa air supply, and then allowed to rest for 1 second. Data was collected by the single board real-time controller, reconfigurable IO Module (sbRIO) and transferred to the computer. This process was repeated until the actuator pressure exceeded 620 kPa. Then the exhaust valve was opened for 10 ms repeatedly in 1 second

A

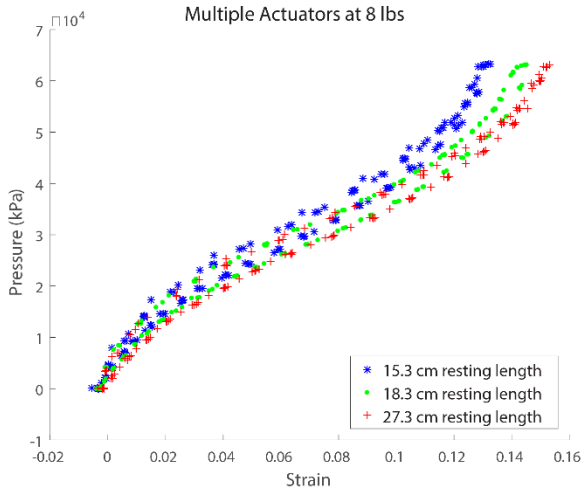

B

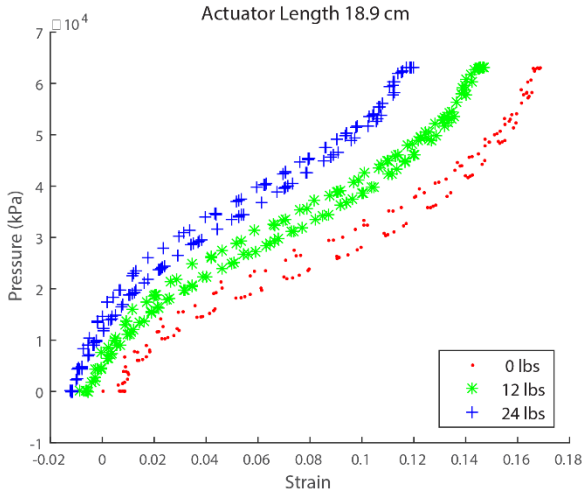

Figure 3. Data for multiple actuators cycled between 0 kPa and 620 kPA multiple times. A) Three different actuators with 8 lbs attached to the end. Although most models do not account for end effects it is apparent that initial actuator length has a significant effect on the strain of the actuator. B) One actuator with multiple weights attached at the end. It is apparent that a change in force both shifts and modifies the shape of the curve. The initial length and force effects are accounted for in our model.

intervals with data taken at each increment until the actuator returned to 0 gauge pressure. This was repeated for a total of 300 data recordings. This procedure was performed while hanging a weight ranging from 0 to 25 lbs. (0-11.34 kg) in 1 lb. (0.45 kg) increments. Each data point was associated with actuator dimensions, weight, pressure, and length at the time of recording.

Actuator Model

The Festo fluidic muscle is a McKibben type actuator but with the cross weave of fibers woven into the bladder membrane rather than being external to the tube as in a typical McKibben. Many physics based models have been developed ([35] for review), however there are often still errors resulting from initial actuator length inaccuracy, internal actuator friction, and end effects. Another approach is to fit a large parameter set with multiple polynomial terms [34], however this makes it difficult to understand the important factors involved and can result in over fitting of the data. The approach we used in this work was to analyze the data and make equation choices that fit data trends with as few parameters that we thought possible. A sample of the data can be seen in Fig. 3.

The data show that end effects are significant at both low and high pressure zones such that pressure vs. strain resembles a tangent function but offset from 0, such that $P \cong a_0 + a_1 * \tan(a_2 k + a_3)$ where k is the strain and a_i are constants to be determined. This curve was observed for all actuator lengths, however because end effects are more significant with shorter actuators, the width of the curve depends strongly on the maximum contraction each actuator achieved (Fig. 3A). The strain at 620 kpa, hereafter referred to as maximum strain, can be used in the equation to stretch or contract the curve. The maximum strain, k_{max}, is the only parameter which must be found experimentally for new actuators and is calculated by:

$$\boldsymbol{k_{max} = \frac{L_{rest} - L_{620\,kpa}}{L_{rest}}} \quad (1)$$

where L_{rest} is the resting length of the actuator and L_{620} is its length measured when it is inflated to 620kpa. By placing k_{max} in the denominator of the tangent, the curve is scaled such that lower maximum strain causes the curve to contract compared to an actuator with a higher maximum strain:

$$\boldsymbol{P \cong a_0 + a_1 * tan(a_2(\frac{k}{k_{max}}) + a_3)} \quad (2)$$

Force has two major effects on the pressure vs. strain curve. The first indicates a linear proportionality in which the central point of the curve is shifted. The second shows a contracting of the tangent curve with increased end effector force such that:

$$\boldsymbol{P \cong a_0 + a_1 * tan\left(a_2\left(\frac{k}{a_4 * F + k_{max}}\right) + a_3\right) + a_5 * F} \quad (3)$$

Finally, the hysteresis from internal friction results in a constant offset based on filling or emptying air from the actuator. This constant offset can be modeled using a binary term, *S*, and the final model for pressure as a function of strain and force is:

$$\boldsymbol{P = a_0 + a_1 * tan\left(a_2\left(\frac{k}{a_4 * F + k_{max}} + a_3\right)\right) + a_5 * F + a_6 * S} \quad (4)$$

Where a_0 through a_6 are constants that were solved for to fit the data. Parameter fitting was performed on three of the actuators (15.31, 19.50, and 28.09 cm lengths) and validated on the other three (18.28, 18.94, and 27.27 cm lengths).

The model equation is nonlinear with three terms inside the tangent function, making it impossible to solve for all values

using a least squares fit of the data. Therefore, a Nelder-Mead simplex method was used to determine the parameter values [36]. The Nelder-Mead simplex method was initialized with a least squares linear regression fit for terms a_1 through a_4 with terms $a_5 = 2$, $a_6 = 0$ and $a_7 = -0.5$. Then random perturbations of up to 100% were done from these initial values and used to initialize the Nelder-Mead simplex method. The optimization reduced the rms error between the calculated pressure and experimentally determined pressures. The Nelder-Mead method was run until either the linear distance in the simplex or the normalized error was less than machine epsilon. The process was repeated 5 times with the previous best fit as the new starting point.

Robot Testing and Control

The model was applied to control the actuators on the front right leg of Puppy (Fig. 4), a four legged robot with three planar degrees of freedom per leg first introduced in [24]. Each joint has two antagonistic actuators and a joint angle sensor (Vishay Spectrol 140-0-0-103). Each actuator has separate input (Matrix 758 Vacuum) and exhaust valves (Matrix 859) with a pressure sensor (Freescale MPX5700GP) in parallel with the actuator. A feedforward controller using this model is used to control each of the joints on the front right leg. The actuators used for the model fit are the elbow flexor, elbow extensor, and shoulder extensor. The same model was then applied to the wrist extensor, wrist flexor and shoulder flexor.

To validate the accuracy of the actuator model, we tested the ability of the robot to track specific joint angles while applying different torques. Actuator strain is calculated from the angle by:

$$\boldsymbol{k} = \frac{\boldsymbol{l_{rest} - l_{angle}}}{\boldsymbol{l_{rest}}} \quad (5)$$

Where $\boldsymbol{l_{angle}}$ is

$$\boldsymbol{l_{angle} = l_0 + l_1\, cos(\alpha + \theta)} \quad (6)$$

Where $\boldsymbol{l_0}$, $\boldsymbol{l_1}$, and $\boldsymbol{\alpha}$ are constants calculated for each joint based on the geometry of the attachment points of the muscle around the joint and $\boldsymbol{\theta}$ is the desired joint angle. Force is calculated from torque by:

$$\boldsymbol{F} = \frac{\boldsymbol{T}}{\boldsymbol{d\, cos(\beta + \theta)}} \quad (7)$$

Where $\boldsymbol{d}$ is the length from the joint to the muscle's lower attachment point, $\boldsymbol{\beta}$ is the offset which causes $\boldsymbol{cos(\beta + \theta) = 1}$ when the muscle is at 90 degrees from the joint, and $\boldsymbol{T}$ is the desired torque.

A feedforward controller built from these models was implemented in Labview 2014 and run on the sbRIO. As shown in Fig. 5, the computer commands angles (α) with desired torques (T). Desired actuator strain (k) and force (F) are calculated and input to the actuator model to compute pressure.

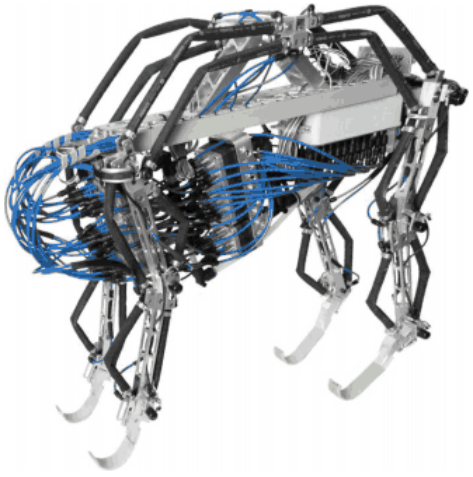

Figure 4. Puppy robot with Festo actuators. Overtime, permanent kinks have developed in the actuators which result in poor modeling under combined low load and low pressure conditions. Modeling and model testing was performed using actuators in the front right leg.

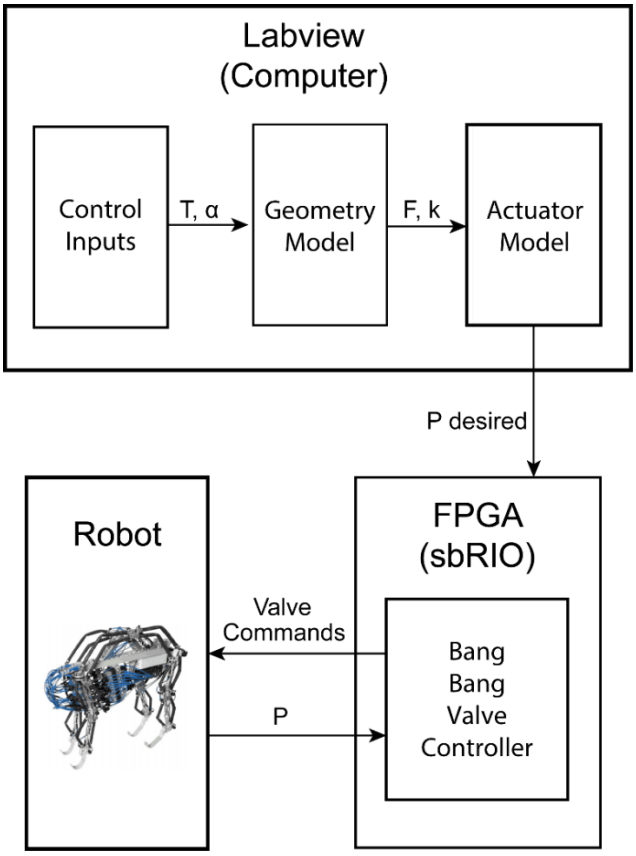

Figure 5. Control flow diagram for actuators. The user commands desired angle and torque for the different joints. Desired strain and force for the individual actuators are calculated based on robot and actuator geometry. These values are then input to the actuator model to determine actuator pressure. On the FPGA, this desired pressure is compared to the current pressure and the appropriate valves are opened and closed until the measured pressure is within ±17 kPa of the desired pressure.

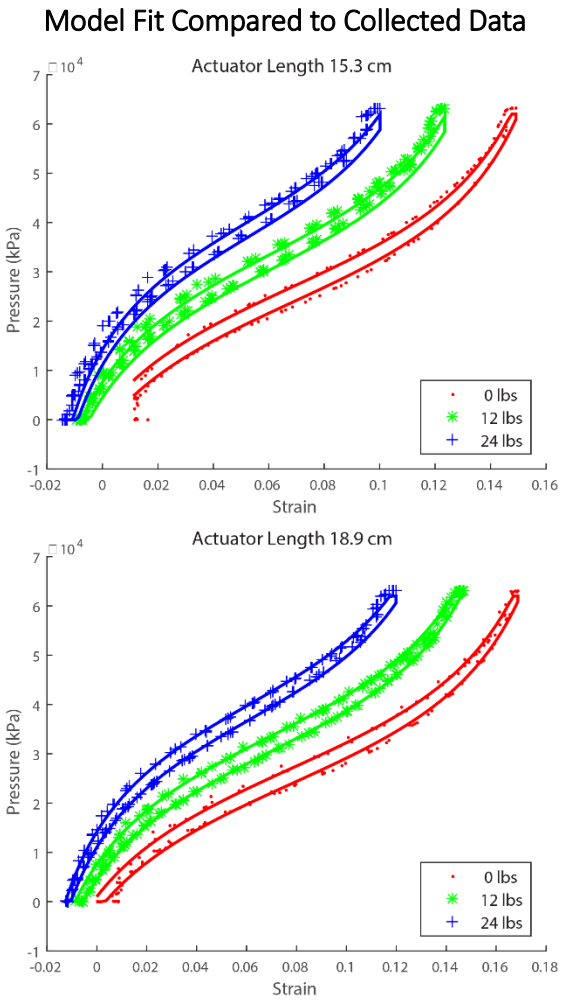

Figure 6. Two comparisons of the model fit with the collected data. The elbow extensor (length 15.3 cm) actuator was used in developing the model while the wrist extensor (length 18.9) was not. The elbow extensor fit has the most error compared to all other actuators compared. The largest error is due to the kink (see Fig. 4) which only effects the combined low pressure and low force case.

For testing purposes, two muscles are controlled to the same commanded angle, and are given equal and opposite torques to balance the joint. This control module provides the desired pressure for each muscle to the valve controller, which is run on a field-programmable gate array (FPGA). The valve controller performs bang-bang control by opening the required inlet or exhaust valves until the desired pressure is reached. The bandwidth on this lowest level of valve control is able to maintain the pressure within the actuators to within approximately ±15 kPa of the desired value.

Each joint is provided a series of command angles from the computer and the actual angles are recorded as the controller works to provide the desired pressures based on the actuator model. This is repeated for desired torques of 0, 1, and 2 N-m. The desired torque is applied to both antagonistic joint actuators at the same time. This increases the force that each actuator is applying to the joint, increasing the stiffness of the joint.

RESULTS

Actuator Model

The Nelder-Mead method resulted in values for Eq. 4 shown in Table I. This fit has an root mean square (rms) error of 11.17 kPa and a maximum error of 75.8 kPa. This is an rms error of 1.8% with a maximum error of 12.2%. Fig. 6 shows the model fit with the data collected at 0, 12 lbs (5.44 kg), and 24 lbs (10.88 kg) on a muscle on which the fit was performed (15.31 cm), and one for which it was not (18.94 cm). The average and maximum errors for each individual actuator are reported in Table II.

a_0 kPa	a_1 kPa	a_2	a_3	a_4 $1/_{mN}$	a_5 $(\mathrm{kPa}/_{mN})$	a_6 kPa
254.3	192.0	2.0265	-0.461	-0.331	1.230	15.6

Table I: Parameters in Equation (1) found through optimization fit of the data collected from three of the six actuators.

Length (cm)	RMS (kPa)	Max Error (kPa)
15.3	16.9	75.8
18.3	11.4	75.8
18.9	7.4	48.0
19.5	14.5	65.5
27.3	8.3	39.3
28.1	8.6	71.4

Table II: Error between model and data collected for each actuator.

Robot Control

The FPGA and valve response time is able to control the pressure within the actuators to within approximately ± 15 kPa. This is above the rms error in all but one of the actuators in the model, indicating that the model is, in general, more accurate than a realized controller can be for this system. To compensate, a ± 17 kPa no-control buffer zone is used around the desired pressure of each actuator. That is, if the measured pressure is within 17 kPa of the commanded pressure, no control action takes place. Both actuators in the elbow were used in the control model, and one actuator in the shoulder. For all three joints, when commanded to a series of specific angles, the controller is able to stably control the robot to different control angles within 2 degrees of accuracy under no torque (Fig. 7). Note that there is no control feedback of joint angle, only feedback control of desired pressure. When torque is commanded, control of the elbow drifts in more flexed positions. This is expected from inspecting the model of the elbow extensor and seeing that the model predicts lower pressures than is necessary to hold a specific strain. The shoulder control remains within 3 degrees under load, though more drifting occurs at more extended angles. Despite the fact that the wrist has no actuators which were used in determining the model, it has the most accurate control.

The ability of the controller to respond to dynamic signals is also tested. Because there is no inertia model built into the controller, the wrist joint is used to minimize effects of lag and overshoot.

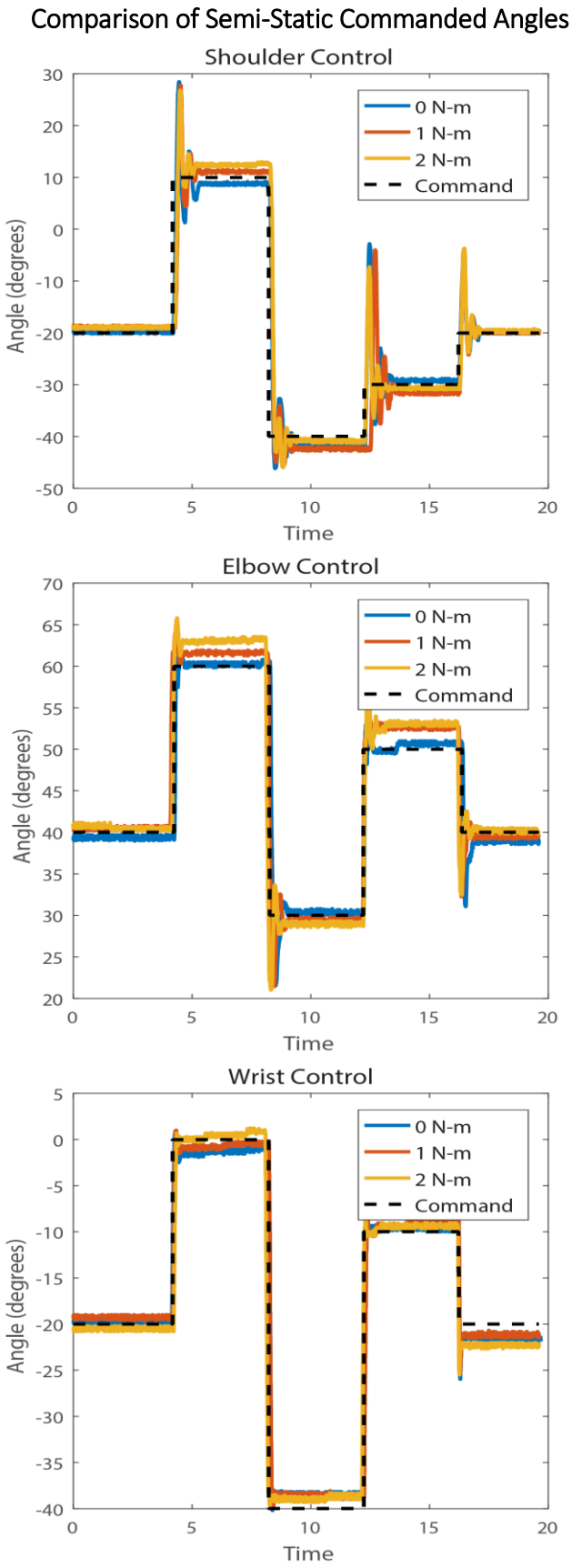

Figure 7. Controller accuracy for producing desired angles from pressure control based on the model. Torques are applied by antagonistic muscles situated across each joint. For all joints, the feedforward calculated steady state pressure values are able to control the joints to within 3 degrees of the desired angle. The controller does not account for limb dynamics and does not attempt to control pressure fill rate. Limb inertia accounts for the large overshoots visible in joints with large limb masses distal to the joint.

Different frequency sine waves are commanded to the wrist angle and the ability of the controller to follow the commands is shown in Fig. 8.

DISCUSSION

Actuator Model

The model fits actuators of different lengths. The model is able to capture the effect that the resting length and attachment hardware has on actuator strain (Fig. 5) with the inclusion of the maximum strain variable into the equation. This makes control possible for a new robot without the need for taking a great deal of data and doing a fit for each new actuator. Only two lengths must be measured for each new actuator and the model is complete. Fig. 6 shows two example fits, and it can be seen that even the worst fit (elbow extensor) matches the data shape well.

The model is least accurate when there is combined low pressure and low force. This is an artifact of the actuators on this robot which have permanent kinks in them (Fig. 4). These kinks keep them from stretching out fully without applying force in this state. This is most readily visible with the elbow extensor where there is no change in length in the collected data when the pressure is less than 50 kPa.

Robot Control

Control of semi-static joint positioning is accurate within three degrees, and is well within the range of joint variation seen during walking in animal systems. This accuracy holds for different opposing torques on the joint as well, indicating that force control of the muscles is possible. When the angle position is fed back into the robot then only the desired force must be specified to determine the desired pressure. This enables the robot to be controlled with specified torque or muscle activations such as in [17].

This also enables the implementation of a low impedance controller. When the current angle is used as the desired angle and no force is desired, a human operator can move the joints by hand with little resistance from the robot. No joint torques or force on the arm need be computed for this to occur. The actuator compliance allows for small changes in angle with little force. These new angles are then used to compute new desired pressures to keep the actuators at the desired length for the new angles. When the operator is done moving the robot arm, the joints maintain their position and do not drift.

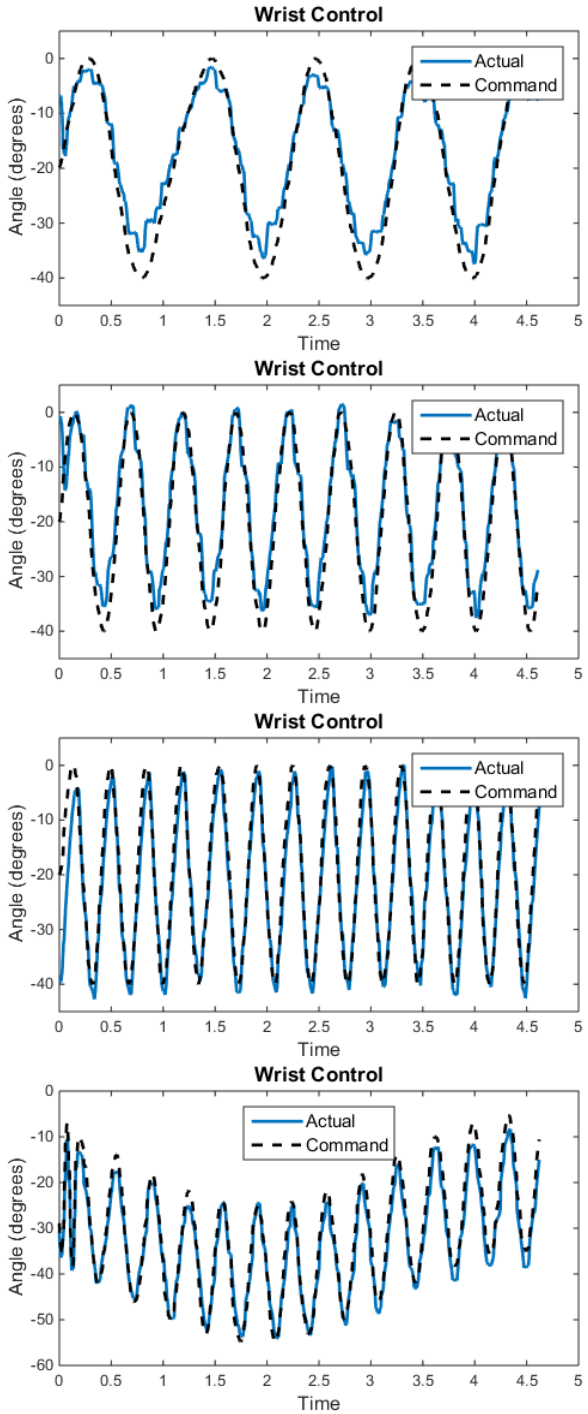

Figure 8. Wrist joint follows different frequency sine waves. Because the actuators do not fully empty, the controller is able to trace sine waves at varied mean points at higher frequencies.

This ability of the actuators to follow joint movements without applying torques decreases actuator response times to new commands in opposite directions. Previous controllers on the robot required that an actuator be fully emptied to ensure it did not provide counter torques to a movement. When the actuator is required to provide a force, time is spent filling up the empty actuator before it can provide the commanded force. With the actuator model, responses to directional changes can be performed more rapidly. This is readily noticeable in Fig. 8 where the controller is able to cycle 30 degrees of rotation at 3 Hz over a range of mean set points.

There are two main reasons for the angle overshoot. The first, most readily seen in the shoulder control is that of angular momentum. No dynamic model is built into the controller, therefore no attempt is made to slow the arm down or create a smooth trajectory. Second, foam is placed in the air line in series with the pressure sensors. This foam low-pass filters pressure readings, however it creates a delay in the actual pressure readings. This delay causes the valves to stay open longer than desired, needing a corrective action from the opposing valve to bring the actuator to the correct pressure. Though not related to the actuator model, an intelligent pressure rate fill model could feasibly be included to reduce this overshoot and improve performance.

The model provides sufficient accuracy for use in legged robotics while only requiring the collection of two easily acquired values for each actuator. This greatly increases the applicability of these actuators as actuator lengths can be tailored to specific project or robot without requiring impractical measurements or sacrificing control.

CONCLUSIONS

We developed an empirical model in which the pressure of Festo MXAM-10-AA actuators are described as a function of strain, maximum actuator strain, stretching\contracting state, and applied force. This model is effective for different length actuators and can be used to develop feedforward control without needing to perform additional tests beyond determining the resting length and minimum contraction length of new actuators. The model fills a gap between simpler models, which do not account for end effects that are significant at shorter lengths, and more complex models, which are not generalizable and require significant data capture for each actuator in use. The effectiveness of the model has been demonstrated on three revolute joints with 6 different actuators on the front leg of a robot. We expect that the model could be extended to Festo fluidic muscles of different diameters in future work.

ACKNOWLEDGEMENTS

The authors would like to thank Matthew Klein for significant help with learning Labview programming.

REFERENCES

1. Alexander RM. Alternative Land Locomotion in Principles of Animal Locomotion. 2003.
2. Jindrich DL, Full RJ. Dynamic stabilization of rapid hexapedal locomotion. J Exp Biol. 2002;205 Pt 18:2803–23. http://www.ncbi.nlm.nih.gov/pubmed/12177146.
3. Loeb E, Brown E, Cheng J. A hierarchical foundation for models of sensorimotor control. Exp Brain Res. 1999;126:1–18.
4. Blickhan R. The spring-mass model for running and hopping. J Biomech. 1989.
5. McMahon T a, Cheng GC. The mechanics of running: how does stiffness couple with speed? J Biomech. 1990;23 Suppl 1:65–78.

6. Farley CT, Houdijk HH, Van Strien C, Louie M. Mechanism of leg stiffness adjustment for hopping on surfaces of different stiffnesses. J Appl Physiol. 1998;85:1044–55.
7. Ferris DP, Liang K, Farley CT. Runners adjust leg stiffness for their first step on a new running surface. J Biomech. 1999;32 March:787–94.
8. Pratt GA, Williamson MM. Series elastic actuators. In: Intelligent Robots and Systems 95.'Human Robot Interaction and Cooperative Robots', Proceedings. 1995 IEEE/RSJ International Conference on. IEEE; 1995. p. 399–406. http://ieeexplore.ieee.org/xpls/abs%7B_%7Dall.jsp?arnumber=525827.
9. Ham VR, Sugar TG, Vanderborght B, Hollander KW, Lefeber D. Compliant actuator designs: Review of actuators with passive adjustable compliance/controllable stiffness for robotic applications. IEEE Robot Autom Mag. 2009;16 September:81–94.
10. Webster VA, Leibach R, Hunt AJ, Bachmann RJ, Quinn RD. Design and control of a tunable compliance actuator. In: Biomimetic and Biohybrid Systems. 2014. p. 344–55. doi:10.1007/978-3-319-09435-9_30.
11. Colbrunn RW, Nelson GM, Quinn RD. Modeling of Braided Pneumatic Actuators for Robotic Control. In: International Conference on Intelligent Robots and Systems. 2001.
12. Hunt AJ, Schmidt M, Fischer MS, Quinn RD. Neuromechanical Simulation of an Inter-leg Controller for Tetrapod Coordination. In: Biomimetic and Biohybrid Systems - Living Machines 2014. 2014. p. 142–53.
13. Szczecinski NS, Martin JP, Quinn RD, Ritzmann RE. Modeling Mantis Prey Tracking with Head, Prothoracic, and Thoracic Movements. In: International Congress of Neuroethology. 2014. p. 2011.
14. Tóth TI, Knops S, Daun-Gruhn S. A neuromechanical model explaining forward and backward stepping in the stick insect. J Neurophysiol. 2012;107:3267–80. doi:10.1152/jn.01124.2011.
15. Schilling M, Hoinville T, Schmitz J, Cruse H. Walknet, a bio-inspired controller for hexapod walking. Biol Cybern. 2013;107:397–419.
16. Gay S, Santos-Victor J, Ijspeert AJ. Learning robot gait stability using neural networks as sensory feedback function for Central Pattern Generators. 2013 IEEE/RSJ Int Conf Intell Robot Syst. 2013;:194–201. doi:10.1109/IROS.2013.6696353.
17. Hunt AJ, Szczecinski NS, Andrada E, Fischer MS, Quinn RD. Using Animal Data and Neural Dynamics to Reverse Engineer a Neuromechanical Rat Model. In: Biomimetic and Biohybrid Systems - Living Machines 2015. Wilson SP, Verschure PFMJ, Mura A, Prescott TJ, editors. Barcelona, Spain; 2015. p. 211–22.
18. Tytell E, Holmes P, Cohen AH. Spikes alone do not behavior make: why neuroscience needs biomechanics. Curr Opin Neurobiol. 2011;:1–7. doi:10.1016/j.conb.2011.05.017.
19. Gaylord R. Fluid Actuated Motor System and Stroking Device. 1958.
20. Shadow Robot Company. http://www.shadowrobot.com/products/air-muscles/.
21. Klute GK, Czerniecki JM, Hannaford B. McKibben artificial muscles: pneumatic actuators with biomechanical intelligence. 1999 IEEE/ASME Int Conf Adv Intell Mechatronics (Cat No99TH8399). 1999;:221–6. doi:10.1109/AIM.1999.803170.
22. Inoue K. Rubbertuators and Applications for Robots. In: Robotics Research. Tokyo, Japan; 1987. p. 57–63.
23. Kingsley DA, Quinn RD, Ritzmann RE. A Cockroach Inspired Robot With Artificial Muscles. 2006 IEEE/RSJ Int Conf Intell Robot Syst. 2006;:1837–42. doi:10.1109/IROS.2006.282229.
24. Aschenbeck KS, Kern NI, Bachmann RJ, Quinn RD. Design of a Quadruped Robot Driven by Air Muscles. In: The First IEEE/RAS-EMBS International Conference on Biomedical Robotics and Biomechatronics, 2006. BioRob 2006. Ieee; 2006. p. 875–80. doi:10.1109/BIOROB.2006.1639201.
25. Minh TV, Kamers B, Ramon H, Van Brussel H. Modeling and control of a pneumatic artificial muscle manipulator joint – Part I: Modeling of a pneumatic artificial muscle manipulator joint with accounting for creep effect. Mechatronics. 2012;22:923–33. doi:10.1016/j.mechatronics.2012.06.002.
26. Tondu B, Lopez P. Modeling and control of McKibben artificial muscle robot actuators. Control Syst IEEE. 2000;:15–38. http://ieeexplore.ieee.org/xpls/abs%7B_%7Dall.jsp?arnumber=833638.
27. Ahn KK, Thanh TDC. Nonlinear PID control to improve the control performance of the pneumatic artificial muscle manipulator using neural network. J Mech Sci Technol. 2005;19:106–15. http://link.springer.com/article/10.1007/BF02916109.
28. Caldwell DG, Medrano-Cerda GA, Goodwin M. Control of pneumatic muscle actuators. IEEE Control Syst Mag. 1995;15:40–8. doi:10.1109/37.341863.
29. Colbrunn RRW, Nelson GM, Quinn RD. Design and control of a robotic leg with braided pneumatic actuators. In: International Conference on Intelligent Robots and Systems. Case Western Reserve University; 2001. p. 141. doi:10.1109/IROS.2001.976298.
30. Vanderborght B, Ham R Van, Daerden F, Lefeber D, Van Damme M, Verrelst B. Proxy-based Sliding Mode Control of a Planar Pneumatic Manipulator. Int J Rob Res. 2009;28:266–84.
31. Andrikopoulos G, Nikolakopoulos G. Piecewise affine modeling and constrained optimal control for a pneumatic artificial muscle. IEEE Trans Ind Electron. 2014;61:904–16. http://ieeexplore.ieee.org/xpls/abs%7B_%7Dall.jsp?arnumber=6484956.
32. Szepe T. Accurate force function approximation for pneumatic artificial muscles. 3rd IEEE Int Symp Logist Ind Informatics. 2011;:127–32. doi:10.1109/LINDI.2011.6031134.
33. Sárosi J. New model for the force of fluidic muscles. Proc Fact Autom. 2012;:7–12. http://csuka.mk.u-szeged.hu/%7B~%7Dsarosi/function1.pdf.
34. Hošovský A, Havran M. Dynamic Modeling of One Degree of Freedom Pneumatic Muscle-Based. Teh Vjesn. 2012;19:673–81. doi:681.523.5:004.896.
35. Kelasidi E, Andrikopoulos G, Nikolakopoulos G, Manesis S. A survey on pneumatic muscle actuators modeling. 2011 IEEE Int Symp Ind Electron. 2011;:1263–9. doi:10.1109/ISIE.2011.5984340.
36. Nelder J, Mead R. A simplex method for function minimization. Comput J. 1965;:308–13.